

Planck Constraints on Holographic Dark Energy

Miao Li,^{1,2,3,*} Xiao-Dong Li,^{4,†} Yin-Zhe Ma,^{5,6,‡} Xin Zhang,^{7,8,§} and Zhenhui Zhang^{1,2,3,¶}

¹*Institute of Theoretical Physics, Chinese Academy of Sciences, Beijing 100190, China*

²*Kavli Institute for Theoretical Physics China,
Chinese Academy of Sciences, Beijing 100190, China*

³*Key Laboratory of Frontiers in Theoretical Physics,
Chinese Academy of Sciences, Beijing 100190, China*

⁴*Korea Institute for Advanced Study, Hoegiro 87,
Dongdaemun-Gu, Seoul 130-722, Republic of Korea*

⁵*Department of Physics and Astronomy, University of British Columbia, Vancouver, V6T 1Z1, BC Canada*

⁶*Canadian Institute for Theoretical Astrophysics,
60 St. George Street Toronto, M5S 3H8, Ontario, Canada*

⁷*College of Sciences, Northeastern University, Shenyang 110004, China*

⁸*Center for High Energy Physics, Peking University, Beijing 100080, China*

Abstract

We perform a detailed investigation on the cosmological constraints on the holographic dark energy (HDE) model by using the *Planck* data. We find that HDE can provide a good fit to the *Planck* high- ℓ ($\ell \gtrsim 40$) temperature power spectrum, while the discrepancy at $\ell \simeq 20 - 40$ found in the Λ CDM model remains unsolved in the HDE model. The *Planck* data alone can lead to strong and reliable constraint on the HDE parameter c . At the 68% confidence level (CL), we obtain $c = 0.508 \pm 0.207$ with *Planck*+WP+lensing, favoring the present phantom behavior of HDE at the more than 2σ CL. By combining *Planck*+WP with the external astrophysical data sets, i.e. the BAO measurements from 6dFGS+SDSS DR7(R)+BOSS DR9, the direct Hubble constant measurement result ($H_0 = 73.8 \pm 2.4 \text{ km s}^{-1} \text{ Mpc}^{-1}$) from the *HST*, the SNLS3 supernovae data set, and Union2.1 supernovae data set, we get the 68% CL constraint results $c = 0.484 \pm 0.070$, 0.474 ± 0.049 , 0.594 ± 0.051 , and 0.642 ± 0.066 , respectively. The constraints can be improved by 2%–15% if we further add the *Planck* lensing data into the analysis. Compared with the *WMAP*-9 results, the *Planck* results reduce the error by 30%–60%, and prefer a phantom-like HDE at higher significant level. We also investigate the tension between different data sets. We find no evident tension when we combine *Planck* data with BAO and *HST*. Especially, we find that the strong correlation between $\Omega_m h^3$ and dark energy parameters is helpful in relieving the tension between the *Planck* and *HST* measurements. The residual value of $\chi^2_{Planck+WP+HST} - \chi^2_{Planck+WP}$ is 7.8 in the Λ CDM model, and is reduced to 1.0 or 0.3 if we switch the dark energy to w model or the holographic model. When we introduce supernovae data sets into the analysis, some tension appears. We find that the SNLS3 data set is in tension with all other data sets; for example, for the *Planck*+WP, *WMAP*-9 and BAO+*HST*, the corresponding $\Delta\chi^2$ is equal to 6.4, 3.5 and 4.1, respectively. As a comparison, the Union2.1 data set is consistent with these three data sets, but the combination Union2.1+BAO+*HST* is in tension with *Planck*+WP+lensing, corresponding to a large $\Delta\chi^2$ that is equal to 8.6 (1.4% probability). Thus, combining internal inconsistent data sets (SNIa+BAO+*HST* with *Planck*+WP+lensing) can lead to ambiguous results, and it is necessary to perform the HDE data analysis for each independent data sets. Our tightest self-consistent constraint is $c = 0.495 \pm 0.039$ obtained from *Planck*+WP+BAO+*HST*+lensing.

PACS numbers: 98.80.-k, 95.36.+x.

*Electronic address: mli@itp.ac.cn

†Electronic address: xiaodongli@kias.re.kr

‡Electronic address: mayinzhe@phas.ubc.ca

§Electronic address: zhangxin@mail.neu.edu.cn

¶Electronic address: zhangzh@itp.ac.cn

I. INTRODUCTION

Since the discovery of the cosmic acceleration [1], dark energy has become one of the most important research areas in modern cosmology [2]. From the last decade, although a variety of dark energy models have been proposed to explain the reason of cosmic acceleration, the physical nature of dark energy is still a mystery.

The dark energy problem may be in essence an issue of quantum gravity [3]. It is commonly believed that the holographic principle is a fundamental principle of quantum gravity [4]. Based on the effective quantum field theory, Cohen *et al.* [5] suggested that quantum zero-point energy of a system with size L should not exceed the mass of a black hole with the same size, i.e., $L^3 \Lambda^4 \leq LM_{\text{Pl}}^2$ (here $M_{\text{Pl}} \equiv 1/\sqrt{8\pi G}$ is the reduced Planck mass, and Λ is the ultraviolet (UV) cutoff of the system). In this way, the UV cutoff of a system is related to its infrared (IR) cutoff. When we consider the whole universe, the vacuum energy related to this holographic principle can be viewed as dark energy, and therefore the holographic dark energy density becomes

$$\rho_{\text{de}} = 3c^2 M_{\text{Pl}}^2 L^{-2}, \quad (1)$$

where c is a dimensionless model parameter which modulates the dark energy density [6]. In [6], Li suggested that the IR length-scale cutoff should be chosen as the size of the future event horizon of the universe, i.e.,

$$L = a \int_t^{+\infty} \frac{dt}{a}. \quad (2)$$

This leads to such an equation of state of dark energy

$$w_{\text{de}}(z) = \frac{1}{3} - \frac{2}{3c} \sqrt{\Omega_{\text{de}}(z)}, \quad (3)$$

which satisfies $w_{\text{de}} \approx -0.9$ for $\Omega_{\text{de}} = 0.7$ and $c = 1$. Thus, an accelerated expanding universe can be realized in this model. In Eq. (3), the function $\Omega_{\text{de}}(z)$ is determined by the following coupled differential equation system

$$\frac{1}{E(z)} \frac{dE(z)}{dz} = -\frac{\Omega_{\text{de}}(z)}{1+z} \left(\frac{1}{c} \sqrt{\Omega_{\text{de}}(z)} + \frac{1}{2} - \frac{\Omega_r(z) + 3}{2\Omega_{\text{de}}(z)} \right), \quad (4)$$

$$\frac{d\Omega_{\text{de}}(z)}{dz} = -\frac{2\Omega_{\text{de}}(z)(1 - \Omega_{\text{de}}(z))}{1+z} \left(\frac{1}{c} \sqrt{\Omega_{\text{de}}(z)} + \frac{1}{2} + \frac{\Omega_r(z)}{2(1 - \Omega_{\text{de}}(z))} \right), \quad (5)$$

where $E(z) \equiv H(z)/H_0$ is the dimensionless Hubble expansion rate, and $\Omega_r(z) = \Omega_r(1+z)^4/E(z)^2$. Note that in this paper we only consider a spatially flat universe. The initial conditions are $E(0) = 1$ and $\Omega_{\text{de}}(0) = 1 - \Omega_c - \Omega_b - \Omega_r$.

The holographic dark energy (HDE) model described above is a viable and physically plausible dark energy candidate, as an alternative to the standard cosmological constant model (Λ). The model has been widely studied both theoretically [7] and observationally [8]. The data used in these works mainly include the type Ia supernovae (SNIa), baryon acoustic oscillations (BAO), the direct measurement of Hubble constant, and the Cosmic Microwave Background (CMB) data from the *Wilkinson Microwave Anisotropy Probe* (*WMAP*). These works show that the HDE model can provide a good fit to the data, and $c < 1$ is favored by the data. For example, a recent analysis reports the 68% confidence level (CL) constraint $c = 0.680^{+0.064}_{-0.066}$ from *WMAP-7+SNIa+BAO+HST* [9].

In this March, the European Space Agency (ESA) and the *Planck* Collaboration publicly released the CMB data based on the first 15.5 months of *Planck* operations, along with a lot of scientific results [10]. They show that the standard six-parameter Λ CDM model provides an extremely good fit to the *Planck* spectra at high multipoles, while there are some discrepancy at $\ell \simeq 20-40$. Some cosmological parameters, e.g., n_s , Ω_k , and N_{eff} , are measured with unprecedented precision. Interestingly, the *Planck* values for some Λ CDM parameters are significantly different from those previously measured. For the matter density parameter, the *Planck* data give $\Omega_m = 0.315 \pm 0.017$ (68% CL) [11]. This value is higher than the *WMAP-7* result $\Omega_m = 0.273 \pm 0.030$ [12] and the *WMAP-9* result $\Omega_m = 0.279 \pm 0.025$ [13], and is in tension with the SNLS3 result $\Omega_m = 0.211 \pm 0.069$ [14]. For the Hubble constant, *Planck* gives a low value $H_0 = 67.3 \pm 1.2 \text{ km s}^{-1} \text{ Mpc}^{-1}$, which is in tension with the results of the direct measurements of H_0 , i.e., $H_0 = 73.8 \pm 2.4 \text{ km s}^{-1} \text{ Mpc}^{-1}$ reported by Riess *et al.* [15], and $H_0 = 74.3 \pm 1.5$ (statistical) ± 2.1 (systematic) $\text{km s}^{-1} \text{ Mpc}^{-1}$ reported by Freedman *et al.* [16]. The discrepancy is at about the 2.5σ level. They also show that, the *Planck* constraints of Ω_m and H_0 , although are in tension with SNLS3 and *HST* observations, are in agreement with the geometrical constraints from BAO surveys [11].

The *Planck* data also improve the constraints on dark energy [11]. Actually, the results can be significantly different if the *Planck* data are combined with different astrophysical data sets. For a constant w model (here after, w CDM model), the *Planck* results give $w = -1.13^{+0.13}_{-0.10}$ and $w = -1.09 \pm 0.17$ (95% CL) by using CMB combined with BAO and Union2.1 [17] data, respectively, which are consistent with the cosmological constant. However, when combined with SNLS3 data and H_0 measurement, the results are $w = -1.13^{+0.13}_{-0.14}$ and $w = -1.24^{+0.18}_{-0.19}$ (2σ CL), respectively, favoring $w < -1$ at the $1-2\sigma$ level. For a dynamical equation of state $w = w_0 + w_a(1 - a)$, the results from the *Planck*+WP+BAO and *Planck*+WP+Union2.1 data combinations are in agreement with a cosmological constant, while the *Planck*+WP+ H_0 and *Planck*+WP+SNLS3 (here, WP represents the *WMAP-9* polarization data) results are in tension with $w = -1$ at the more than 2σ level.

Based on the arrival of a bunch of new data sets, it is very important to re-analyze the HDE model in

light of *Planck* and *WMAP* 9-year data. This will enable us to answer a lot of interesting questions: What are the constraint results of the cosmological parameters in the HDE model from the *Planck* data? What is the difference between the fitting results of *Planck* and *WMAP*? What are the results if we combine the *Planck* data with the BAO, SNIa, and *HST* data? Whether are they consistent or in tension with each other? Since the Hubble constant H_0 is correlated with the HDE parameter c , can HDE help us to relax the tension between the *Planck* data and the direct measurements of H_0 ? Since a phantom dark energy can reduce the TT power spectrum amplitude at large scales, can HDE help us to relieve the mismatches between theoretical and observational power spectra at $\ell \simeq 20 - 40$? The *Planck* temperature power spectrum showed anomalous fitting results of the lensing parameter A_L in the Λ CDM model (i.e., $A_L > 1$), can HDE help us to remove or relieve this “anomaly”? The main task of this paper is to find firm, reliable answers to these stimulating questions.

This paper is organized as follows. In Sec. II, we give a brief introduction to the data used in this work and our method of data analysis. In Sec. III, we present and compare the fitting results of HDE by using the CMB-only data of *Planck* and *WMAP*-9. In Sec. IV, we combine the CMB data with the external astrophysical data sets including BAO, SNLS3, Union2.1 and *HST*, and discuss the fitting results and the tensions. Some concluding remarks are given in Sec. V. In this work, we assume today’s scale factor $a_0 = 1$, so the redshift z satisfies $z = 1/a - 1$. We use negative redshifts to represent the future; in this way, $z = -1$ corresponds to the infinite future when $a \rightarrow \infty$. The subscript “0” indicates the present value of the corresponding quantity unless otherwise specified.

II. DATA ANALYSIS METHODOLOGY

To analyze the HDE, we modify the CAMB package [18] to incorporate the background equations of the HDE model. Furthermore, to investigate the dark energy perturbations, we apply the “parameterized post-Friedmann” (PPF) approach [19]. This method of dealing with dark energy perturbations has been widely used by *WMAP* [12, 13] and *Planck* teams [11]. In our previous work of HDE data analysis [9], we have already employed this method into our pipeline.

The same as [11], we sample cosmological parameter space with Markov Chain Monte Carlo (MCMC) method with the publicly available code COSMOMC [20]. For each analysis, we execute about 8–16 chains until they are converged, satisfying the standard Gelman and Rubin criterion $R - 1 < 0.01$ [21]. To make sure that the tails of the distribution are well enough explored, we also check the convergence of confidence limits with the setting `MPI_Limit_Converge = 0.025` in COSMOMC.

The base Λ CDM model has the standard “six-parameter” as

$$P = \{\Omega_b h^2, \Omega_c h^2, 100\theta_{MC}, \tau, n_s, \ln(10^{10} A_s)\}, \quad (6)$$

where $\Omega_b h^2$ and $\Omega_c h^2$ are the current density of baryon and cold dark matter, respectively, $100\theta_{MC}$ is 100 times the approximation to r_s/D_A in COSMOMC ($r_s = r_s(z_{\text{drag}})$ is the comoving size of sound horizon at baryon-drag epoch, and D_A is the angular diameter distance), τ is the Thomson scattering optical depth due to reionization, n_s is the scalar spectrum index at the pivot scale $k_0 = 0.05 \text{ Mpc}^{-1}$, $\ln(10^{10} A_s)$ is the log power of the primordial curvature perturbations at k_0 .

In the following, we will also discuss the holographic dark energy model and the w CDM model, each of which has an extra parameter to describe the dynamic evolution of dark energy. For HDE model, the extra parameter is c , as described in Eq. (1), and for w CDM model, the extra parameter is w . Therefore, when we compare Λ CDM model with w CDM and HDE models, we should bear in mind that we are comparing a model with 6 parameters with models with 7 parameters.

To make our results comparable with the results of the *Planck* Collaboration, baselines and priors for the parameters in our analysis are adopted same as [11]. In our MCMC chains, these parameters are varied with uniform priors, within the ranges listed in Table 1 of [11]. The range of c is [0.001, 3.5], which is wide enough for covering the physically interesting region. Additionally, a “hard” prior [20, 100] $\text{km s}^{-1} \text{ Mpc}^{-1}$ is imposed to the Hubble constant ¹. The same as [11], we assume a minimal-mass normal hierarchy for the neutrino masses by setting a single massive eigenstate $m_\nu = 0.06 \text{ eV}$.

Cosmological data used in this work fall into two parts: the CMB data from *Planck* and *WMAP*, and the other data sets including BAO, SNIa and H_0 . We introduce them in the following two subsections.

A. CMB data

The CMB data based on the first 15.5 months of *Planck* operations are publicly released by the ESA and *Planck* Collaboration in March 2013 [10]. At the same time, the *Planck* likelihood softwares are also made publicly downloadable. ² The likelihood software provided by the *Planck* Collaboration includes the following four parts:

- The high- ℓ temperature likelihood CamSpec. At $\ell = 50 - 2500$, a correlated Gaussian approximation is employed to obtain the likelihood, based on a fine-grained set of angular cross-spectra derived from multiple detector combinations between the 100, 143, and 217 GHz frequency channels.

¹ In the MCMC, samples with H_0 out of this range are rejected.

² <http://pla.esac.esa.int/pla/aio/planckProducts.html>

- The low- ℓ temperature likelihood. At $\ell < 50$, the likelihood exploits all *Planck* frequency channels from 30-353 GHz, separating the CMB signal from the diffuse Galactic foregrounds through a physically motivated Bayesian component separation technique.
- The low- ℓ polarization likelihood. The present *Planck* data release includes only temperature data, and the *Planck* Collaboration supplements the *Planck* likelihood with the 9-year *WMAP* (*WMAP*-9) polarization likelihood derived from the *WMAP* polarization maps at 33, 41, and 61 GHz (K, Q, and V bands).
- The *Planck* lensing likelihood. Lensing is detected independently in *Planck* 100, 143, and 217 GHz channels with an overall significance of greater than 25σ [22]. The gravitational lensing data are good at constraining dark energy through the lensing effect coming from the distortion of the large scale structure that emerged after $z = 10$ (at this stage, the universe is dark energy dominated).

In the following context, we will use “*Planck*” to represent the *Planck* temperature likelihood (including both the low- ℓ and high- ℓ parts), “WP” to represent the *WMAP* polarization likelihood as a supplement of *Planck*, and “lensing” to represent the likelihood of *Planck* lensing data.

To study the difference between the fitting results by using *Planck* and *WMAP* data, in this work we also perform the analysis of HDE by using *WMAP*-9 data. The data and likelihood software are downloadable at the Legacy Archive for Microwave Background Data Analysis (LAMBDA).³ We will not use the high-resolution CMB data of the Atacama Cosmology Telescope and the South Pole Telescope [23]. They are not publicly available in the current version of COSMOMC package, and only marginally affect the fitting results compared with *Planck* or *WMAP*-9.

B. External astrophysical data sets

The CMB data alone are not powerful in constraining dark energy parameters, since dark energy affects the late time cosmic evolution. When combined with the external astrophysical data sets (hereafter, “Ext” or “Exts”), CMB data are helpful in breaking the degeneracies between parameters and improving the constraints on dark energy parameters [24]. In our analysis, we will consider the following four Exts:

- The BAO data can provide effective constraints on dark energy from the angular diameter distance–redshift relation. In our analysis, similar to [11], we use the following data sets, the 6dF Galaxy Survey $D_V(0.106) = (457 \pm 27)\text{Mpc}$ [25] (D_V is a distance indicator similar to angular diameter

³ <http://lambda.gsfc.nasa.gov>

distance D_A , see Eq. (46) in [11]), the reanalyzed SDSS DR7 BAO measurement $D_V(0.33)/r_s = 8.88 \pm 0.17$ [26], and the BOSS DR9 measurement $D_V(0.57)/r_s = 13.67 \pm 0.22$ [27]. SDSS DR7 and BOSS DR9 are the two most accurate BAO measurements, and the correlation between the surveys is a marginal effect to the parameter estimation.

- The direct measurement of the Hubble constant, $H_0 = 73.8 \pm 2.4 \text{ km s}^{-1} \text{ Mpc}^{-1}$ (1σ CL) [15], from the supernova magnitude–redshift relation calibrated by the *HST* observations of Cepheid variables in the host galaxies of eight SNe Ia. Here the uncertainty is 1σ and includes known sources of systematic errors.
- The Union2.1 compilation [17], consisting of 580 SNe, calibrated by the SALT2 light-curve fitting model [28].
- The SNLS3 “combined” sample [14], consisting of 472 SNe, calibrated by both SiFTO [29] and SALT2 [28]. For simplicity, we do not consider the SNLS3 compilation calibrated separately by SiFTO or SALT2.

In the following context, we will use “BAO”, “*HST*”, “Union2.1” and “SNLS3” to represent these four Exts. We will also use “SNIa” to represent a supernovae data set, either Union2.1 or SNLS3.

III. CMB-ONLY RESULTS

TABLE I: CMB-only fitting results of the HDE model.

Data	Ω_m		c		H_0		$-\ln \mathcal{L}_{max}$
	Best fit	68% limits	Best fit	68% limits	Best fit	68% limits	
<i>Planck</i>	0.142	0.261 ± 0.097	0.301	0.587 ± 0.449	100.00	77.34 ± 12.82	3894.4
<i>Planck</i> +lensing	0.150	0.248 ± 0.084	0.317	0.531 ± 0.296	96.80	78.51 ± 12.09	3899.8
<i>Planck</i> +WP	0.157	0.268 ± 0.100	0.317	0.612 ± 0.433	95.57	75.60 ± 12.83	4902.6
<i>Planck</i> +WP + lensing	0.180	0.248 ± 0.079	0.354	0.508 ± 0.207	88.65	78.36 ± 11.36	4907.3
<i>WMAP</i> -9	0.350	0.401 ± 0.082	0.965	$1.88^{+0.79}_{-1.20}$	62.37	59.57 ± 8.15	3779.0

In this section we present the CMB-only fitting results of the HDE model. The CMB+Ext fitting results are discussed in the next section.

In Table I, we list the fitting results of the HDE model from the CMB data alone. Best-fit values as well as the 68% CL limits for Ω_m , c and H_0 are listed in columns 2–7. The minus log-maximal likelihood

is listed in the last column. The first 4 rows list the results of *Planck*, *Planck*+lensing, *Planck*+WP, and *Planck*+WP+lensing. For comparison, the *WMAP*-9 results are listed in the last row.

In the following two subsections, we firstly introduce the temperature power spectra with the best-fit parameters, and then discuss the constraints on cosmological parameters.

A. Temperature power spectra

In the upper panel of Fig. 1 we show the temperature power spectrum of the best-fit HDE model (green dotted) by using the *Planck*+WP data. As comparisons, best-fit spectra of the Λ CDM model and the w CDM model from *Planck*+WP are also plotted in black solid and red dashed lines. To see the difference between the three spectra, the residuals compared with the best-fit six-parameter Λ CDM model are shown in the lower panel. We find that all the three models can provide a good fit to the *Planck* high- ℓ power spectrum, while at $\ell \simeq 20 - 40$ there are some mismatches, as reported by *Planck* [11]. The HDE model is not helpful in relieving this discrepancy. The main difference among the power spectra of the three models lie in the $\ell \lesssim 20$ region, where we find that amplitudes of HDE and w CDM spectra are lower than the Λ CDM spectrum. This phenomenon is consistent with the result of [9], where it is shown that a phantom-like dark energy component leads to smaller C_ℓ^{TT} at low- ℓ region.

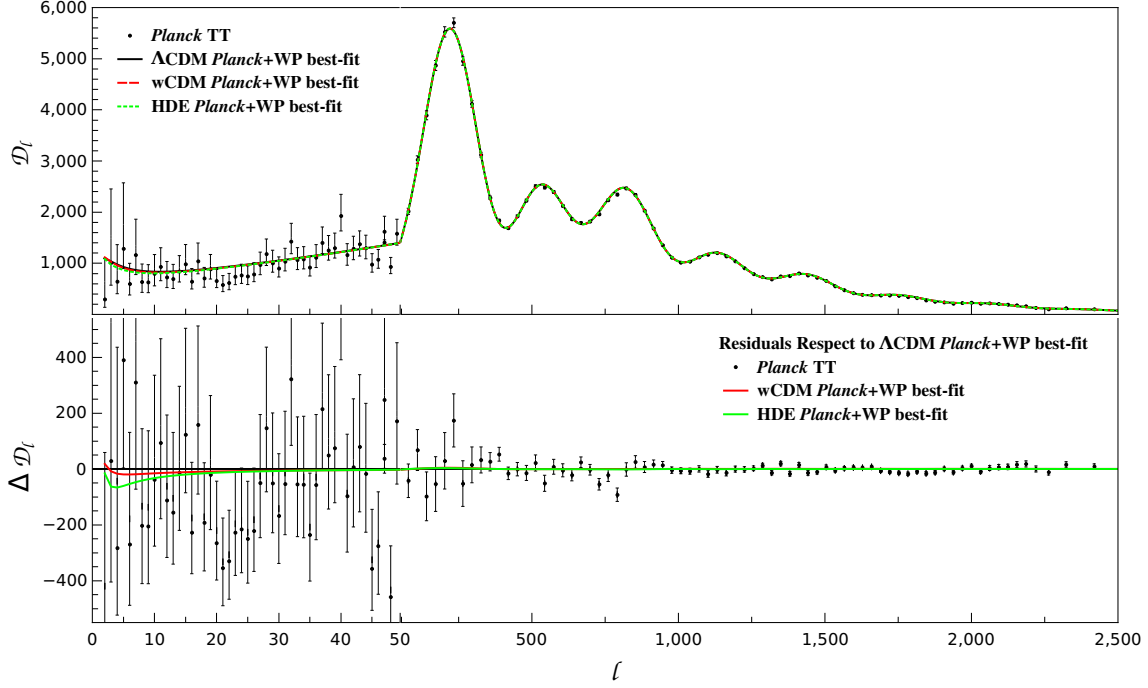


FIG. 1: Upper panel: CMB TT power spectrum plotted with the best-fit parameters of Λ CDM model (black solid), w CDM model (red dashed), and HDE model (green dotted), from the *Planck*+WP data. The ordinate axis shows $\mathcal{D}_\ell \equiv \ell(\ell + 1)C_\ell/2\pi$ in units of μK^2 . The *Planck* binned temperature spectrum is shown in black dots with error bars. Lower panel: Residuals with respect to the temperature power spectrum of the best-fit six-parameter Λ CDM model.

It is also of interest to compare the *WMAP* and *Planck* spectra in the HDE model. The Appendix A of [11] shows some inconsistency between the *Planck* and *WMAP* spectra. It is found that the *WMAP* power spectrum re-scaled by a multiplicative factor of 0.975 agree to remarkable precision with the *Planck* spectrum [11]. Thus, in Fig. 2 we plot the *WMAP*-9 and *Planck*+WP spectra for the Λ CDM (upper panel), w CDM (middle panel) and HDE (lower panel) models. As expected, in all these three models, we find that the *WMAP*-9 power spectrum (with a multiplicative factor 0.975) matches well with the *Planck* power spectrum. The best-fit power spectra of the three models are similar to each other. More interestingly, in all models we find that at $\ell \sim 1600 - 2000$ the theoretical power spectra of *Planck* and *WMAP*-9 have higher amplitudes than the *Planck* data. This scale corresponds to ~ 10 times the scale of galaxy clusters, and this discrepancy may be due to some unclear physics on this scale.

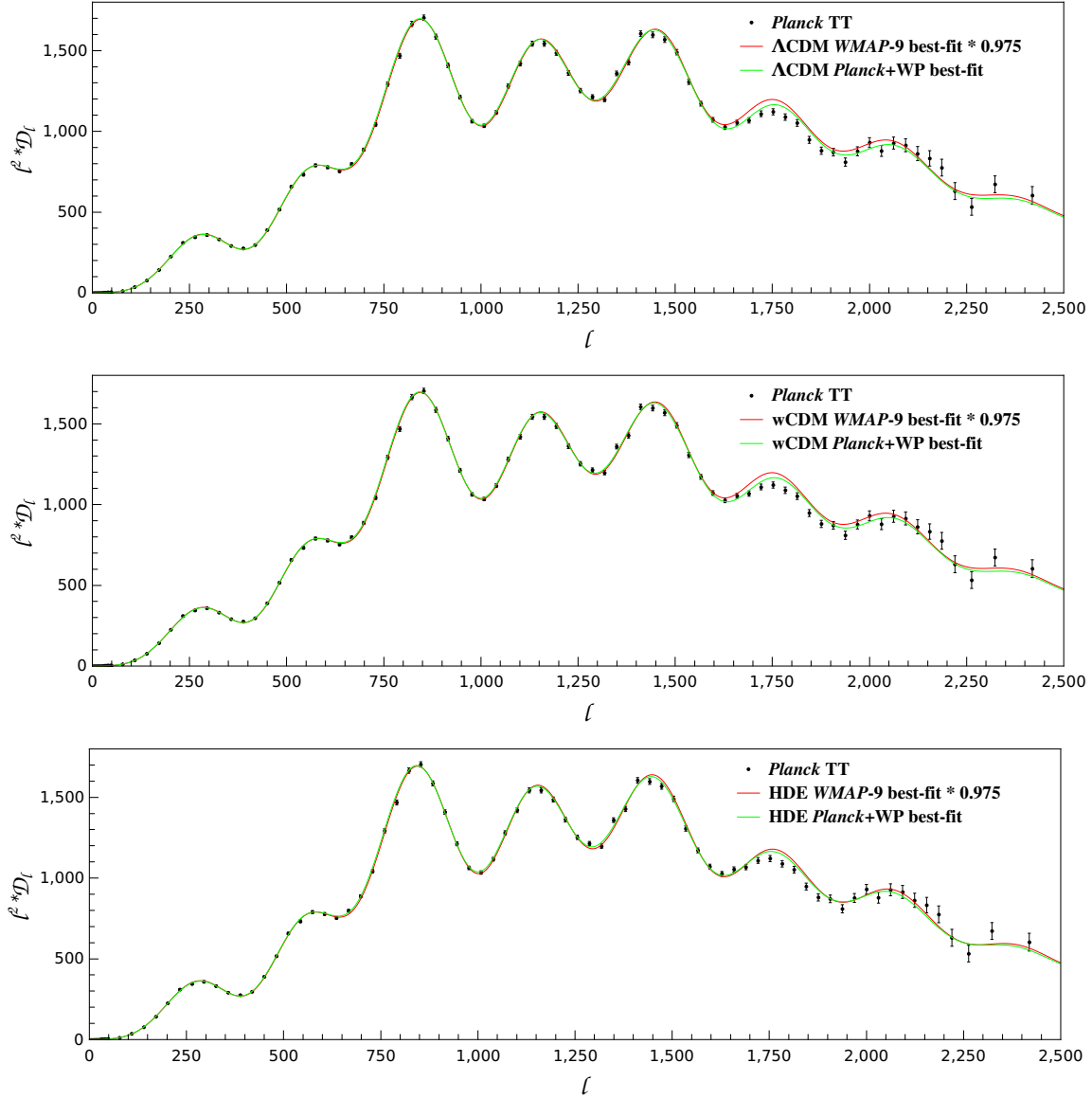


FIG. 2: The *WMAP-9* and *Planck*+WP best-fit power spectra for the Λ CDM (upper panel), w CDM (middle panel) and HDE (lower panel) models. To see the difference between the theoretical power spectra and the observational data at the high- ℓ region, we choose to plot the $\ell^2 \mathcal{D}_\ell$ (in units of mK^2) rather than \mathcal{D}_ℓ . The *Planck*+WP best-fit power spectra are plotted in green lines, and the *WMAP-9* best-fit power spectra multiplied by 0.975 are plotted in red lines. The black points with error bars mark the *Planck* temperature power spectrum data.

B. Constraints on cosmological parameters

In this subsection we discuss the constraints on cosmological parameters in the HDE model.

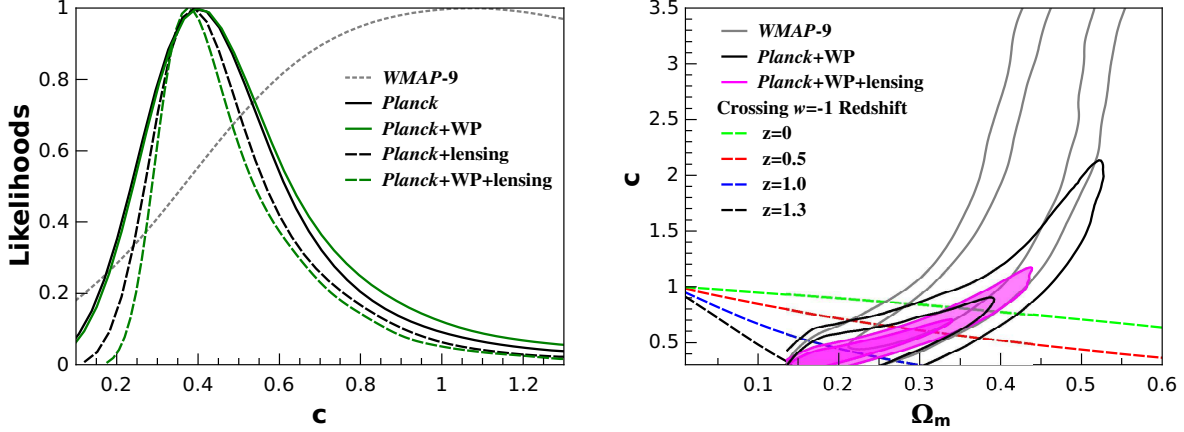


FIG. 3: CMB-only fitting results of the HDE model. Left panel: Marginalized likelihood distributions of c . Right panel: Marginalized 68% and 95% CL contours in the Ω_m - c plane. Dashed lines mark the $w = -1$ crossing at $z = 0, 0.5, 1.0$ and 1.3 .

The likelihood distributions of c are shown in the left panel of Fig. 3. We find that *Planck* data lead to small values of best-fit c , i.e., 0.30–0.35. The 68% CL errors of c are about 0.45 for *Planck* and *Planck*+WP, and are reduced to 0.3 and 0.21 when the lensing data are added. Compared with the *WMAP*-9 alone constraint, $c = 1.786 \pm 0.880$, the *Planck* results reduce the error bar by about 45%–75%. There are clear discrepancies between the mean (see the 68% limits listed in Table I) and the best-fit values of c , implying that the likelihood distribution of c is highly deviated from symmetric form.

The right panel of Fig. 3 shows the Ω_m - c contours of the CMB-only constraints. Results of *WMAP*-9, *Planck*+WP and *Planck*+WP+lensing are plotted. To see the behavior of HDE under the constraints, we also plot the “crossing $w = -1$ redshift” in dashed lines: e.g., parameter space above/below the dashed blue line corresponds to a quintessence/phantom behavior of holographic dark energy at $z = 1.0$. We see that the *WMAP*-9 data alone does not lead to any interesting constraint on c , while the *Planck*+WP results show the preference for $c < 1$ at the 1σ CL. Adding the lensing data tightens the constraint, and the present phantom behavior of holographic dark energy is preferred at the more than 1σ CL. Besides, we find that in the HDE model Ω_m is constrained to be 0.26–0.28 (68% CL) by the *Planck* data, which is smaller than the result in the Λ CDM model. The *WMAP* data alone cannot lead to effective constraint on Ω_m in the HDE model.

The CMB-only constraints on H_0 in the HDE model are listed in the 5th and 6th columns of Table I. Compared with the Λ CDM result, $H_0 = 67.4 \pm 1.4$ (68% CL; *Planck*) [11], the error bars are significantly larger.⁴ Similar phenomenon appears in the *WMAP*-9 results, where we find $H_0 = 59.57 \pm 8.15$ in the HDE

⁴ Since we impose a prior [20, 100] on H_0 in the analysis, the error bars are, actually, under-estimated.

model.

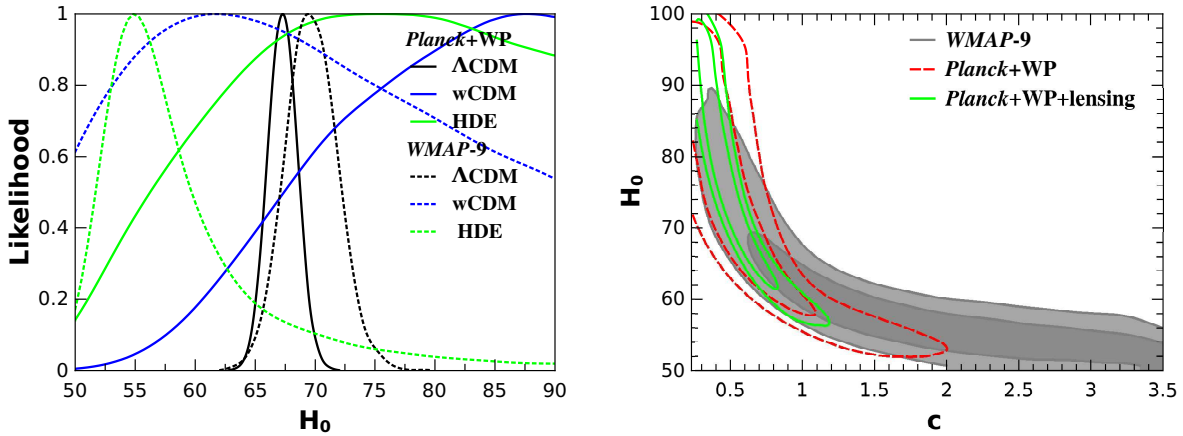


FIG. 4: CMB-only fitting results of the HDE model. Left panel: Marginalized likelihood distributions of H_0 . Right panel: Marginalized 68% and 95% CL contours in the c - H_0 plane.

To make a comparison, in the left panel of Fig. 4 we plot the likelihood distributions of H_0 in the Λ CDM, wCDM and HDE models, constrained by *Planck*+WP and *WMAP*-9 data. We find that, in the Λ CDM model, H_0 is tightly constrained, while in the HDE and wCDM models it cannot be effectively constrained. The right panel shows the c - H_0 contours constrained by *WMAP*-9, *Planck*+WP, and *Planck*+WP+lensing. We see that c and H_0 are strongly anti-correlated with each other. This explains why in the HDE model H_0 cannot be well constrained by CMB-only data.

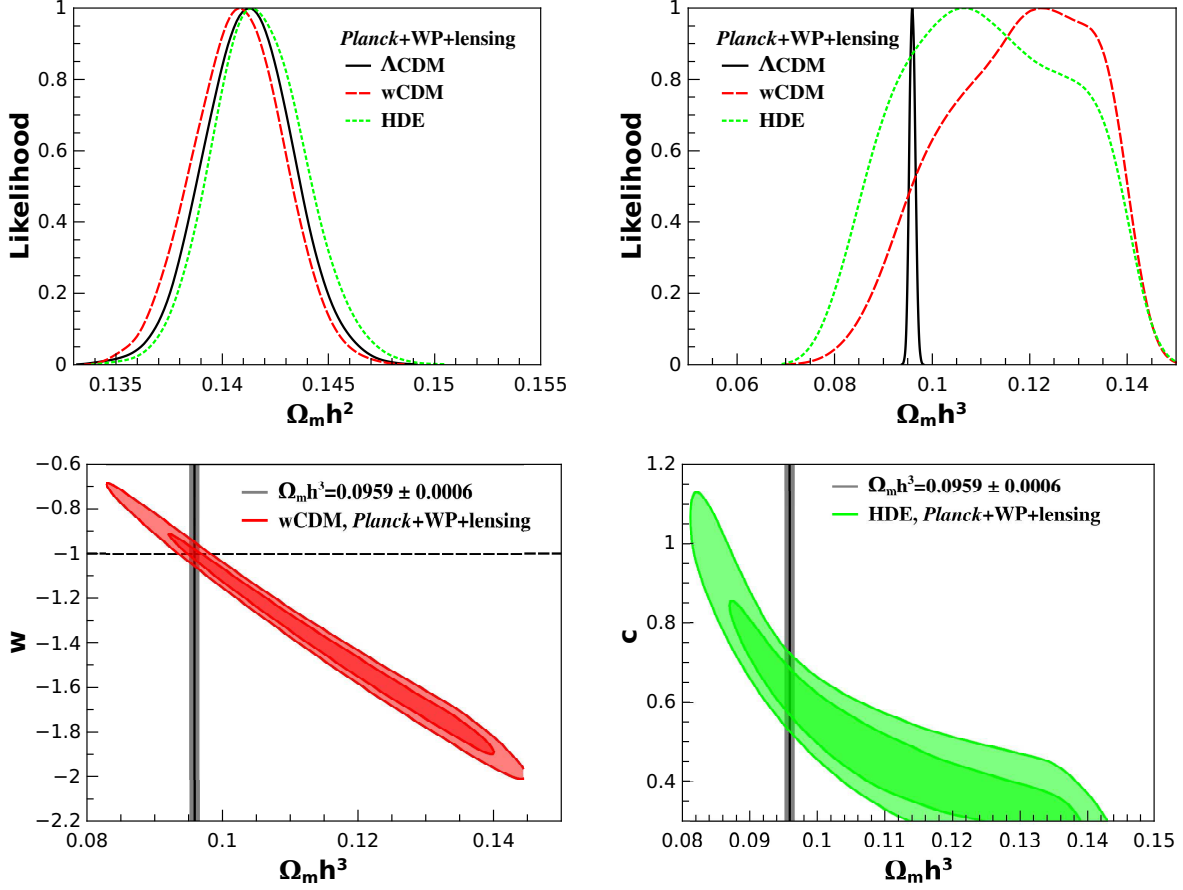


FIG. 5: Upper panel: Marginalized likelihood distributions of $\Omega_m h^2$ and $\Omega_m h^3$, for the Λ CDM (black solid), w CDM (red dashed) and HDE (green dotted) models. Lower panel: Marginalized 68% and 95% CL contours in the $\Omega_m h^3$ - w and $\Omega_m h^3$ - c planes. The gray band marks the constraint $\Omega_m h^3 = 0.0959 \pm 0.0006$ (68% CL; *Planck*) in the Λ CDM model [11].

Furthermore, in order to understand why the likelihood distribution of H_0 is greatly widened in the w CDM and HDE models, in the upper panels of Fig. 5 we plot the likelihood distributions of $\Omega_m h^2$ and $\Omega_m h^3$ in the three models, constrained by *Planck*+WP+lensing. Interestingly, we find similar likelihood distributions of $\Omega_m h^2$ in the three models, but that $\Omega_m h^3$ has much broader distribution in the w CDM and HDE models than in the Λ CDM model. The lower panels show that the above phenomenon is due to the strong anti-correlation between $\Omega_m h^3$ and dark energy parameters. In the Λ CDM model, the precise measurement of acoustic scale in *Planck* leads to a strong constraint on $\Omega_m h^3$, i.e., $\Omega_m h^3 = 0.0959 \pm 0.0006$ (68% CL) [11], (shown as the gray band in the lower panels,) so together with the constraint on $\Omega_m h^2$ we expect a strong constraint on H_0 . However, when we add dark energy parameters like w or c into the analysis, the strong correlation between the parameters makes $\Omega_m h^3$ unconstrained, and so H_0 also becomes unconstrained.

It is expected that the widened H_0 distribution is helpful in relieving the tension between *Planck* and *HST* observations; see [30] for a related work. We will discuss this topic in the next section.

C. CMB lensing parameter A_L

The lensing parameter A_L is defined as a scaling parameter of the lensing potential power spectrum [31],

$$C_\ell^{\phi\phi} \rightarrow A_L C_\ell^{\phi\phi}, \quad (7)$$

and its theoretical expectation is $A_L = 1$. However, by using *Planck*+WP+highL data (“highL” means high- ℓ CMB experiments; see [11] for details), *Planck* Collaboration got $A_L = 1.23 \pm 0.11$ for Λ CDM, showing a 2σ preference for $A_L > 1$ [11]. When adding the lensing measurements into the analysis, the result becomes consistent with $A_L = 1$ at the 1σ level; see Fig. 13 of [11].

To see whether HDE can help to remove this anomaly (i.e., the preference for high A_L in the temperature power spectrum), we repeated the similar analysis and obtained the following results ⁵,

$$A_L = 1.42 \pm 0.19 \text{ (68\% CL; HDE, } Planck + WP), \quad (8)$$

$$A_L = 1.25 \pm 0.15 \text{ (68\% CL; HDE, } Planck + WP + \text{lensing)}. \quad (9)$$

As a comparison, the fitting results in Λ CDM by using the same sets of data are

$$A_L = 1.22 \pm 0.12 \text{ (68\% CL; } \Lambda\text{CDM, } Planck + WP), \quad (10)$$

$$A_L = 1.07 \pm 0.07 \text{ (68\% CL; } \Lambda\text{CDM, } Planck + WP + \text{lensing)}. \quad (11)$$

Corresponding marginalized posterior distributions for A_L are shown in Fig. 6.

⁵ For convenience, in our analysis we did not use the high- ℓ data, which only marginally affect the fitting results of A_L .

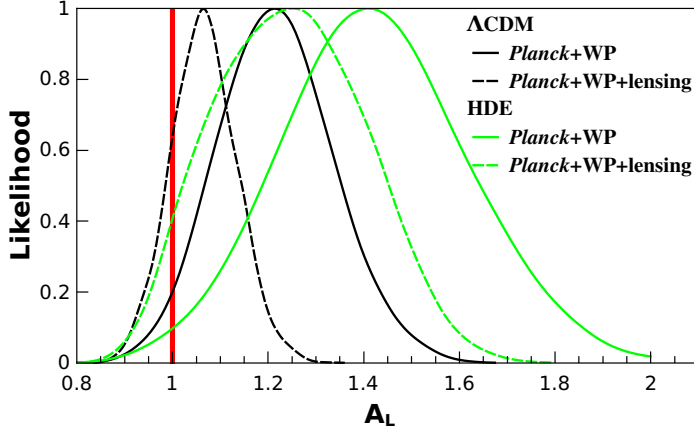


FIG. 6: Marginalized likelihood distributions of the lensing parameter A_L in the Λ CDM (black) and HDE (green) models, by using *Planck*+WP (solid) and *Planck*+WP+lensing (dashed) data. The red solid line marks $A_L = 1$.

Compared with Λ CDM, in the HDE model the error bars of A_L are amplified due to the extra model parameter, but the best-fit values become even larger. As a consequence, we find that $A_L > 1$ at 2.2σ and 1.7σ by using *Planck*+WP and *Planck*+WP+lensing. The anomaly becomes slightly worse than in Λ CDM.

IV. CMB COMBINED WITH ASTROPHYSICAL DATA SET RESULTS

The CMB+Ext fitting results of the HDE model are listed in Table II. Best-fit values as well as 68% CL limits for Ω_m , c and H_0 are listed in the columns 2–7. The maximal likelihood values are listed in the 7th column, and the residual χ^2 values, defined as $\Delta\chi^2_{\text{CMB+Ext}} \equiv \chi^2_{\text{CMB+Ext}} - \chi^2_{\text{CMB}} - \chi^2_{\text{Ext}}$, are listed in the last column. The results from *Planck*+WP combined with external astrophysical data sets are listed in the first nine rows, while the *WMAP*-9 results are listed in the following seven rows. As a comparison, in the last six rows we also list the results from the astrophysical data sets only, including the fitting results of BAO, BAO+*HST*, SNLS3, Union2.1, SNLS3+BAO+*HST*, and Union2.1+BAO+*HST*.

TABLE II: CMB+Ext fitting results of the HDE model.

Data	Ω_m		c		H_0		$-\ln \mathcal{L}_{max}$	$\Delta\chi^2$ ^a
	Best fit	68% limits	Best fit	68% limits	Best fit	68% limits		
<i>Planck</i> +WP + BAO	0.270	0.254 ± 0.024	0.506	0.484 ± 0.070	72.63	75.06 ± 3.82	4903.6	1.7
<i>Planck</i> +WP + BAO + lensing	0.262	0.256 ± 0.022	0.498	0.494 ± 0.062	73.62	74.65 ± 3.39	4908.4	1.9
<i>Planck</i> +WP + <i>HST</i>	0.266	0.257 ± 0.019	0.463	0.474 ± 0.049	73.78	74.77 ± 2.68	4902.8	0.3 ^c
<i>Planck</i> +WP + <i>HST</i> + lensing	0.260	0.256 ± 0.019	0.498	0.489 ± 0.048	73.81	74.62 ± 2.69	4907.9	1.1 ^c
<i>Planck</i> +WP + BAO + <i>HST</i>	0.252	0.255 ± 0.014	0.470	0.481 ± 0.046	75.22	74.75 ± 2.19	4903.6	0.9
<i>Planck</i> +WP + BAO + <i>HST</i> + lensing	0.245	0.255 ± 0.013	0.481	0.495 ± 0.039	75.83	74.5 ± 2.0	4908.5	1.3
<i>Planck</i> +WP + SNLS3	0.300	0.305 ± 0.019	0.584	0.594 ± 0.051	68.81	68.46 ± 1.93	5115.8	6.4
<i>Planck</i> +WP + SNLS3 + lensing	0.310	0.301 ± 0.019	0.610	0.603 ± 0.049	67.73	68.66 ± 1.92	5120.8	7.3
<i>Planck</i> +WP + Union2.1	0.327	0.324 ± 0.021	0.618	0.642 ± 0.066	66.35	66.74 ± 1.94	5176.1	1.6
<i>Planck</i> +WP + Union2.1 + lensing	0.321	0.321 ± 0.021	0.617	0.645 ± 0.063	66.72	66.68 ± 2.03	5181.6	3.4
<i>Planck</i> +WP + SNLS3 + BAO + <i>HST</i> + lensing . .	0.269	0.275 ± 0.011	0.583	0.563 ± 0.035	72.41	71.46 ± 1.37	5123.2	10.9 ^d
<i>Planck</i> +WP + Union2.1 + BAO + <i>HST</i> + lensing .	0.276	0.281 ± 0.012	0.551	0.577 ± 0.039	71.49	70.68 ± 1.40	5185.3	9.6 ^d
<i>WMAP</i> -9 + BAO	0.274	0.284 ± 0.021	0.623	0.746 ± 0.165	70.41	68.93 ± 3.18	3779.6	0.9
<i>WMAP</i> -9 + <i>HST</i>	0.251	0.250 ± 0.020	0.552	0.569 ± 0.086	73.98	73.99 ± 2.71	3779.1	0.2 ^c
<i>WMAP</i> -9 + BAO + <i>HST</i>	0.255	0.259 ± 0.015	0.534	0.567 ± 0.081	73.65	72.96 ± 2.37	3779.7	0.3 ^c
<i>WMAP</i> -9 + SNLS3	0.277	0.280 ± 0.022	0.664	0.696 ± 0.078	69.79	69.44 ± 2.23	3990.6	3.5
<i>WMAP</i> -9 + Union2.1	0.304	0.299 ± 0.023	0.767	0.782 ± 0.105	66.76	67.24 ± 2.18	4051.6	0.1
<i>WMAP</i> -9 + SNLS3 + BAO + <i>HST</i>	0.269	0.270 ± 0.011	0.626	0.645 ± 0.060	70.89	70.89 ± 1.46	3992.2	5.6 ^d
<i>WMAP</i> -9 + Union2.1 + BAO + <i>HST</i>	0.276	0.276 ± 0.011	0.659	0.711 ± 0.074	70.17	69.64 ± 1.37	4054.3	4.3 ^d
BAO	0.227	0.215 ± 0.124	2.391	1.579 ± 0.772	× ^e	×	0.1	--
BAO + <i>HST</i>	0.289	0.332 ± 0.974	0.552	0.666 ± 0.241	73.56	73.49 ± 2.38	0.6	--
SNLS3	0.129	0.118 ± 0.072	1.294	1.519 ± 0.514	×	×	209.8	--
Union2.1	0.256	0.173 ± 0.099	0.024	1.68 ± 0.78	×	×	272.5	--
SNLS3 + BAO + <i>HST</i>	0.294	0.295 ± 0.029	0.612	0.622 ± 0.071	72.27	72.37 ± 2.36	212.5	4.1 ^b
Union2.1 + BAO + <i>HST</i>	0.323	0.326 ± 0.030	0.608	0.633 ± 0.086	73.42	73.09 ± 2.36	273.6	1.0 ^b

$$^a \Delta\chi^2_{\text{CMB+Ext}} \equiv \chi^2_{\text{CMB+Ext}} - \chi^2_{\text{CMB}} - \chi^2_{\text{Ext}}.$$

$$^b \Delta\chi^2_{\text{SNIa+BAO+HST}} \equiv \chi^2_{\text{SNIa+BAO+HST}} - \chi^2_{\text{SNIa}} - \chi^2_{\text{BAO+HST}}.$$

$$^c \Delta\chi^2_{\text{CMB+HST}} \equiv \chi^2_{\text{CMB+HST}} - \chi^2_{\text{CMB}}.$$

$$^d \Delta\chi^2_{\text{CMB+SNIa+BAO+HST}} \equiv \chi^2_{\text{CMB+SNIa+BAO+HST}} - \chi^2_{\text{CMB}} - \chi^2_{\text{SNIa}} - \chi^2_{\text{BAO+HST}}.$$

^e The cross “×” indicates that the parameter is unconstrained by the chosen data sets.

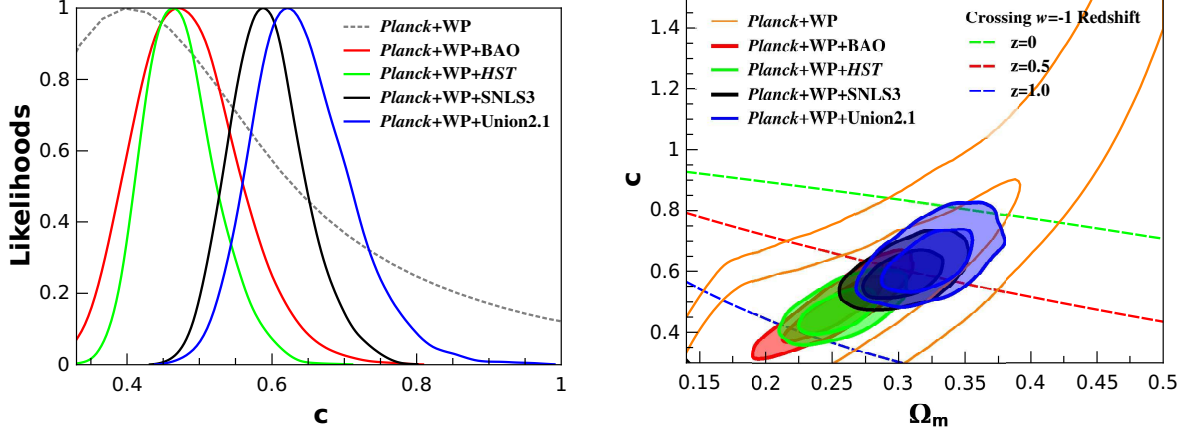


FIG. 7: Fitting results of the HDE model, from *Planck*+WP combined with external astrophysical data sets of BAO (red), *HST* (green), SNLS3 (black) and Union2.1 (blue). Left panel: Marginalized likelihood distributions of c . Right panel: Marginalized 68% and 95% CL contours in the Ω_m - c plane.

We find that adding external astrophysical dataset reduces the error of c to 0.05–0.07. The likelihood distributions of c and the Ω_m - c contours for *Planck*+WP and *Planck*+WP+Ext are plotted in Fig. 7. The best-fit values of c for *Planck*+WP+BAO and *Planck*+WP+HST constraints are around 0.5, while the values for *Planck*+WP+SNLS3 and *Planck*+WP+Union2.1 constraints are around 0.6. As a comparison, the best-fit value of c from *WMAP*-9 combined one Ext is larger, i.e., 0.55–0.77, and the error is also larger, i.e., 0.08–0.17.

We find that the *Planck* lensing data are helpful in improving the constraint on c . By adding the lensing data into the analysis of *Planck*+WP combined with the Ext, such as BAO, *HST*, BAO+*HST*, SNLS3 and Union2.1, the constraint results are improved by 11%, 2%, 15%, 4% and 5%, respectively.

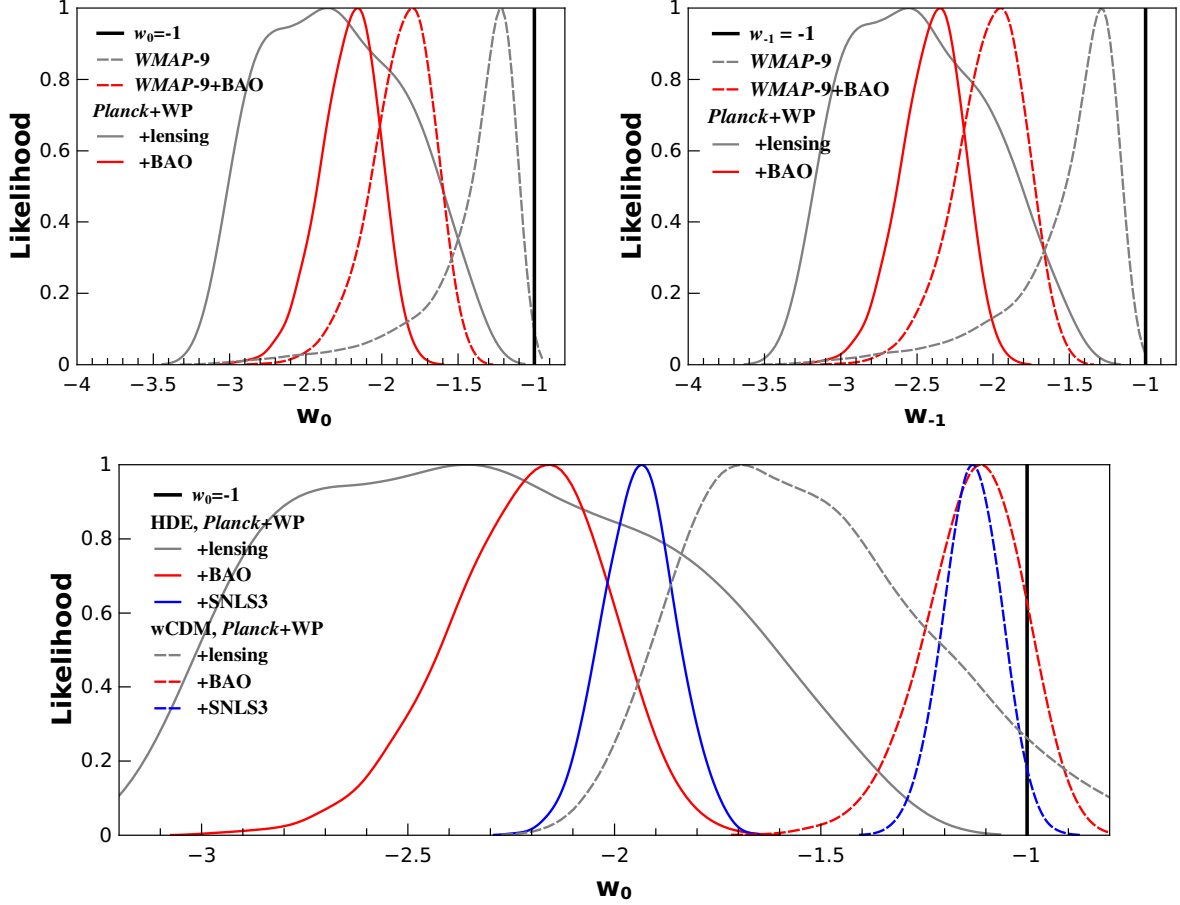


FIG. 8: Marginalized likelihood distributions of dark energy equation of state at $z = 0$ (upper left and lower panels) and $z = -1$ (upper right panel). In the two upper panels, the results of *Planck*+WP combined with lensing (gray solid) and BAO (red solid) are shown. In the lower panel, we also plot the *Planck*+WP+SNLS3 results (blue). The black thick line marks $w = -1$. As comparisons, the *WMAP*-9 (gray dashed) and *WMAP*-9+BAO (red dashed) results are plotted in the two upper panels, and the w CDM results (dashed lines) are plotted in the lower panel.

To see the dynamical behavior of HDE, in Fig. 8 we plot the likelihood distributions of the dark energy equation of state at $z = 0$ (upper left and lower panels) and $z = -1$ (upper right panel). We find that, by using the *Planck* data, a phantom-like holographic dark energy is favored at high confidence level in both current and future epochs. The result of $w_0 < -1$ can be obtained at more than 2σ level by using *Planck*+WP+lensing, even without any Ext combined. These are different from that of the w CDM results (dashed lines in the lower panel), where $w = -1$ is still consistent with the fitting results at a relatively high confidence level.

Furthermore, to investigate the tension between CMB and Ext, in the last column of Table II we list the $\Delta\chi^2$ values for the different combinations. In most combinations we find a small $\Delta\chi^2$, except for

the CMB+SNLS3 results, where $\chi^2_{\text{CMB+SNLS3}} - \chi^2_{\text{CMB}} - \chi^2_{\text{SNLS3}} = 6.4, 7.3,$ and 3.5 for *Planck*+WP, *Planck*+WP+lensing and *WMAP*-9, implying an evident tension. For no-CMB constraints, the result $\chi^2_{\text{SNLS3+BAO+HST}} - \chi^2_{\text{SNLS3}} - \chi^2_{\text{BAO+HST}} = 4.1$ means that SNLS3 is also in tension with BAO+*HST*. The *HST* combined results lead to $\chi^2_{\text{CMB+HST}} - \chi^2_{\text{CMB}} = 1.7, 1.1$ and 0.2 for *Planck*+WP, *Planck*+WP+lensing and *WMAP*-9, implying that there is no severe tension between *HST* and CMB in the HDE model.

In the following, we will discuss the fitting results in detail. We will discuss the fitting results of CMB combined with BAO and *HST* in the first subsection, and the fitting results of CMB combined with SNLS3 and Union2.1 in the second subsection.

A. Combined with BAO and *HST*

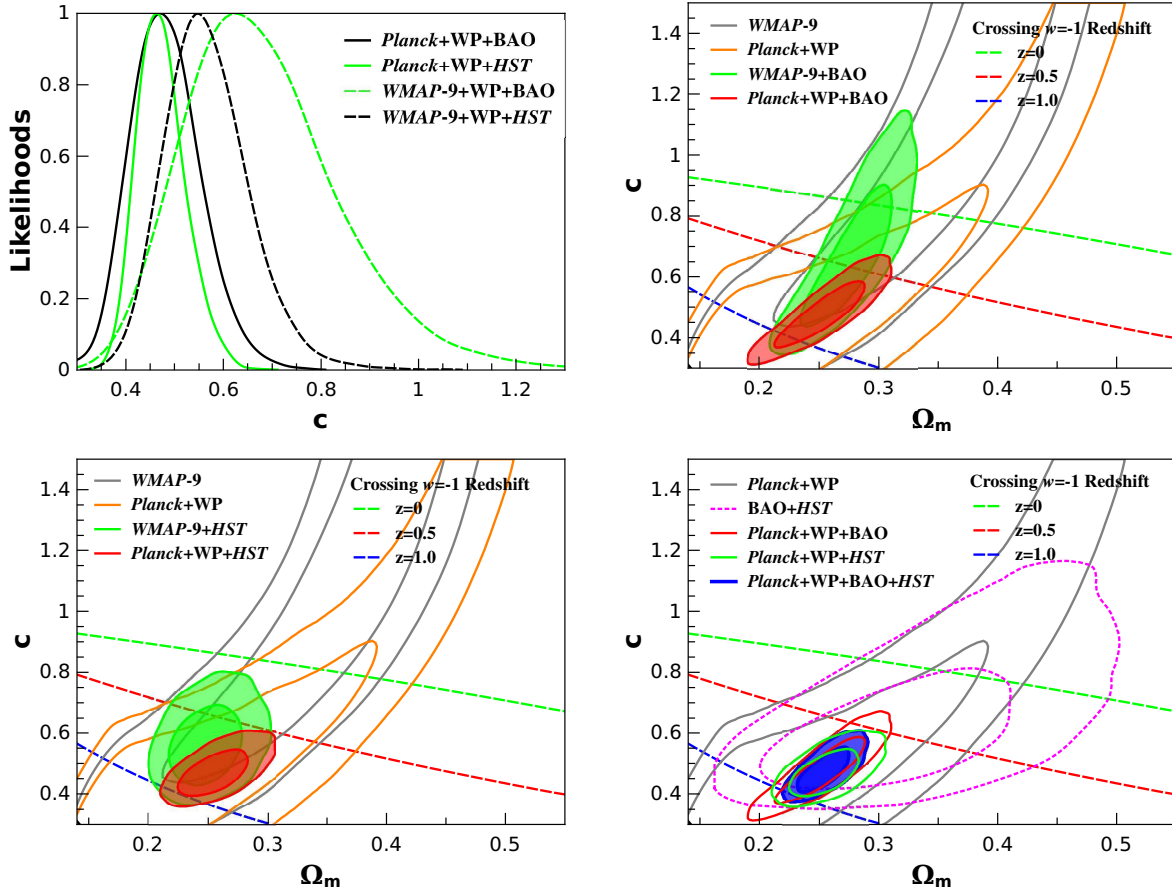


FIG. 9: Fitting results of the HDE model, from CMB combined with BAO and *HST*. The upper-left panel shows the marginalized distributions of c . The other three panels show the marginalized 68% and 95% CL contours in the Ω_m - c plane, including the CMB+BAO results for *Planck* and *WMAP*-9 (upper-right), CMB+*HST* results for *Planck* and *WMAP*-9 (lower-left), and the CMB+*HST*/BAO results for *Planck* (lower-right).

At the 68% CL, we obtain $c = 0.484 \pm 0.070$ (*Planck*+WP+BAO), $c = 0.474 \pm 0.049$ (*Planck*+WP+*HST*), $c = 0.746 \pm 0.165$ (*WMAP*-9+BAO) and $c = 0.569 \pm 0.086$ (*WMAP*-9+*HST*). Compared with the *WMAP*-9 results, the best-fit values of c from the *Planck* data are smaller by 0.1–0.3, and the error bars are reduced by 40%–60%. These results can be seen clearly in the likelihood distributions plotted in the upper-left panel of Fig. 9.

The other three panels of Fig. 9 show the 68% and 95% CL contours in the Ω_m - c plane, including the CMB+BAO results for *Planck* and *WMAP*-9 (upper-right), CMB+*HST* results for *Planck* and *WMAP*-9 (lower-left), and the *Planck*+*HST*/BAO results (lower-right). Interestingly, in the lower-right panel we see that the *Planck*+WP+BAO (red solid) and *Planck*+WP+*HST* (green solid) contours lie in the same position, showing that *Planck*+WP+BAO and *Planck*+WP+*HST* lead to consistent fitting results. This figure also shows a consistent overlap of *Planck*+WP (gray solid) and BAO+*HST* (purple dotted). The combined *Planck*+WP+BAO+*HST* (blue filled region) data lead to a self-consistent constraint, $c = 0.481 \pm 0.046$.

Moreover, we can further tighten the constraints by adding the lensing data into the the analysis. Table II shows that, by adding the lensing data, the *Planck*+WP+BAO constraint on c is improved from 0.484 ± 0.070 to 0.494 ± 0.062 , and the *Planck*+WP+BAO+*HST* result is improved from 0.481 ± 0.046 to $c = 0.495 \pm 0.039$. The error bars are reduced by 12%–15%. The $\Delta\chi^2$ values for the two lensing combined results are 1.9 and 1.3, respectively, showing a good consistency. Actually, the constraint result, $c = 0.495 \pm 0.039$, from *Planck*+WP+BAO+*HST*+lensing is our tightest *self-consistent* constraint on c . If we further add the supernova data set into the analysis, the error bars can be slightly reduced, but a significant inconsistency among the data sets appears. This result also has 35%–50% smaller error bars compared with the *WMAP*-9 all-combined results, where the constraints on c are $c = 0.645 \pm 0.060$ and $c = 0.711 \pm 0.074$ for *WMAP*-9+BAO+*HST* combined with SNLS3 and Union2.1, respectively.

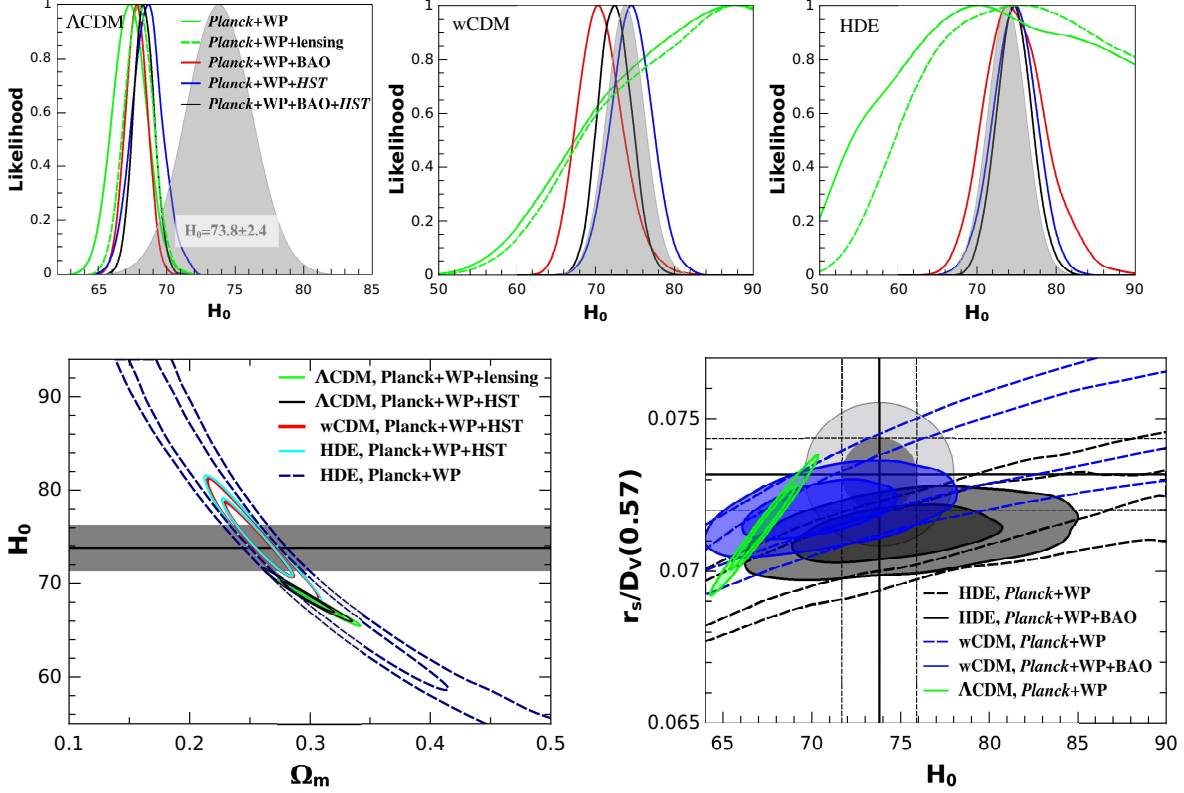


FIG. 10: Upper panels: Marginalized likelihood distributions of H_0 , for the Λ CDM (left panel), w CDM (middle panel) and HDE (right panel) models. The gray filled region represents the *HST* measurement result, $H_0 = 73.8 \pm 2.4$. Lower-left panel: Marginalized 68% and 95% CL contours in the Ω_m – H_0 plane. The gray band shows the result with 1σ range of the *HST* measurement. Lower-right panel: Marginalized 68% and 95% CL contours in the H_0 – $r_s/D_V(0.57)$ plane. The horizontal solid and dashed lines mark the central value and 1σ region of the BOSS DR9 measurement, while the vertical lines mark the observational result of the *HST*. The joint 1 and 2σ likelihood region for BOSS DR9 + *HST* measurements is represented by the dark and light gray shaded contours.

In the last section, we find that in the w CDM and HDE models the CMB-only constraints allow a wide range of H_0 (see Fig. 4). Now, let us see if the tension between CMB and *HST* can be relieved in these two models when the external astrophysical data are added in the analysis. In the upper panels of Fig. 10 we plot the likelihood distributions of H_0 in the Λ CDM (left), w CDM (middle) and HDE (right) models, obtained by using *Planck*+WP (green solid), *Planck*+WP+lensing (green dashed), *Planck*+WP+BAO (red solid), *Planck*+WP+*HST* (blue solid), and *Planck*+WP+BAO+*HST* (black solid), respectively. In all plottings, the *HST* measurement result, $H_0 = 73.8 \pm 2.4$ [15], is shown in the gray filled region. In the upper-left panel, we see that the constraints on H_0 are fairly tight in the Λ CDM model, and the results of various combinations involving *Planck*+WP are all in tension with the *HST* measurement. However, for the w CDM and HDE models, all the CMB combined constraints overlap well with the gray region, showing that the

tension between CMB and *HST* is effectively relieved in these two models if the *Planck* data are combined with BAO or/and *HST*. This phenomenon can be seen more clearly in the Ω_m-H_0 plane for the three models (the lower-left panel). We see that the allowed parameter space of the Λ CDM model is tightly confined by the CMB data, and the positions of *Planck*+WP+lensing (green solid) and *Planck*+WP+*HST* (black solid) contours evidently deviate from the *HST* measurement (the gray band). On the other hand, the CMB data alone cannot effectively constrain the Ω_m-H_0 parameter space for HDE (dark blue dashed). The positions of *Planck*+WP+*HST* contours for the HDE (light blue solid) and w CDM (red solid) models are all well consistent with the *HST* measurement.

TABLE III: Residual χ^2 values in the Λ CDM, w CDM and HDE models

Model	$\chi^2_{Planck+WP+BAO} - \chi^2_{Planck+WP}$	$\chi^2_{Planck+WP+HST} - \chi^2_{Planck+WP}$	$\chi^2_{Planck+WP+BAO+HST} - \chi^2_{Planck+WP}$
Λ CDM	2.5	7.8	9.1
w CDM	2.6	1.0	3.7
HDE	1.9	0.3	1.9

The tension between CMB and the external data sets (e.g., BAO and *HST*) in the HDE model can be characterized by the $\Delta\chi^2$ values, as listed in the last column of Table II. The results are $\Delta\chi^2 = 1.7, 0.3, 0.9, 0.9,$ and 0.2 for *Planck*+WP+BAO, *Planck*+WP+*HST*, *Planck*+WP+BAO+*HST*, *WMAP*-9+BAO, and *WMAP*-9+*HST*, respectively. These values are small, showing that there is no severe tension between the data sets in the HDE model. As a comparison with the w CDM and Λ CDM models, in Table III we show the residuals χ^2 values of *Planck*+WP+BAO, *Planck*+WP+*HST* and *Planck*+WP+BAO+*HST* with respect to *Planck*+WP in the three models. For the Λ CDM model, adding *HST* and BAO+*HST* significantly increases the χ^2 value by 7.8 and 9.1. The increments are 1.0 and 3.7 for the w CDM model, and only 0.3 and 1.9 for the HDE model. Thus, the tension with *HST* measurement is effectively relieved in the two dynamic dark energy models.

Moreover, Fig. 10 and Table III show that there is a better consistency among data sets in the HDE model than in the w CDM model. The best-fit values of H_0 from *Planck*+WP+BAO are 67.63, 69.68 and 72.63 for the Λ CDM, w CDM and HDE models, among which the HDE result is the most close to the *HST* measurement. To understand *why Planck+WP+BAO gives a higher H_0 in the HDE model than in the w CDM model*, in the lower-right panel of Fig. 10 we plot the $H_0-r_s/D_V(0.57)$ contours for the three models. In this figure, we also show the joint 1 and 2σ likelihood region for BOSS DR9 + *HST* measurements in the dark and light gray shaded contours. We see that, for the Λ CDM model, the *Planck*+WP contours (green solid) are consistent with the BOSS DR9 measurement, but are in tension with the *HST* measurement. In the w CDM

and HDE models, the allowed parameter spaces are greatly broadened, and their *Planck*+WP contours (dashed lines) overlap with the gray contours. Interestingly, the positions of the w CDM and HDE contours are different: the HDE contours lie in the smaller $r_s/D_V(0.57)$ region, below the w CDM contours, so they overlap with the gray contours at higher H_0 region. This helps us to understand why the *Planck*+WP+BAO (black filled region) result of the HDE model has higher values of H_0 than the *Planck*+WP+BAO (blue filled region) result of the w CDM model.

Besides, it should be mentioned that, due to the anti-correlation between w (or c) and H_0 , the *Planck*+WP+*HST* leads to phantom results in the w CDM and HDE models. In [11], the *Planck* Collaboration reported a result $w = -1.24^{+0.18}_{-0.19}$ (95% CL, *Planck*+WP+highL+BAO+*HST*) for the w CDM model, which is in tension with $w = -1$ at the more than 2σ level. For the HDE model, the lower-left panel of Fig. 9 shows that the 95% CL contour from *Planck*+WP+*HST* (red filled region) lies below the $z = 0.5$ phantom divide line (red dashed).

B. Combined with SNIa

In this subsection, we discuss the SNIa combined fitting results.

The CMB+SNIa fitting results are plotted in Fig. 11. The likelihood distributions of c are shown in the upper-left panel. At the 68% CL, we get $c = 0.594 \pm 0.051$, $c = 0.642 \pm 0.066$, $c = 0.696 \pm 0.078$ and $c = 0.782 \pm 0.105$ for *Planck*+WP+SNLS3, *Planck*+WP+Union2.1, *WMAP*-9+SNLS3 and *WMAP*-9+Union2.1, respectively. Similar as the above results, compared with the *WMAP*-9 results, the *Planck* results have smaller best-fit values and error bars. Adding lensing into the analysis effectively tightens the constraint, yielding $c = 0.583 \pm 0.042$ and $c = 0.645 \pm 0.063$ for *Planck*+WP+lensing combined with SNLS3 and Union2.1. Compared with CMB+Union2.1, we find that CMB+SNLS3 yields more phantom-like result.

In [11], the *Planck* Collaboration reported that there exists some tension between *Planck* and supernovae data sets, and the tension between *Planck* and SNLS3 is more severe than that between *Planck* and Union2.1. To investigate the tension between CMB and SNIa data sets in the HDE model, in the lower panels we plot the 68% and 95% CL contours in the Ω_m - c plane from *Planck*+WP (orange), *WMAP*-9 (gray), SNIa (blue), *Planck*+WP+SNIa (red filled) and *WMAP*-9+SNIa (green filled). The SNLS3 plottings are shown in the lower-left panel, and the Union2.1 plottings are shown in the lower-right panel. From the positions of the contours, we see that the CMB data are consistent with Union2.1, but in tension with SNLS3 (the 1σ contours of CMB and SNIa do not overlap). Table II shows that $\Delta\chi^2_{Planck+WP+SNIa}$, $\Delta\chi^2_{Planck+WP+lensing+SNIa}$ and $\Delta\chi^2_{WMAP-9+WP+SNIa}$ are 6.4, 7.3 and 3.5 for SNLS3, respectively, while only 1.6, 3.4 and 0.1 for Union2.1,

respectively. Besides, as mentioned above, the results in Table II also show some tension between SNLS3 and BAO+*HST*: for SNLS3 we have $\chi^2_{\text{SNLS3+BAO+HST}} - \chi^2_{\text{SNLS3}} - \chi^2_{\text{BAO+HST}} = 4.1$, while for Union2.1 the value is only 1.0. So, it is fairly remarkable that *for the HDE model the SNLS3 data set is in weak tension with all other data sets.*

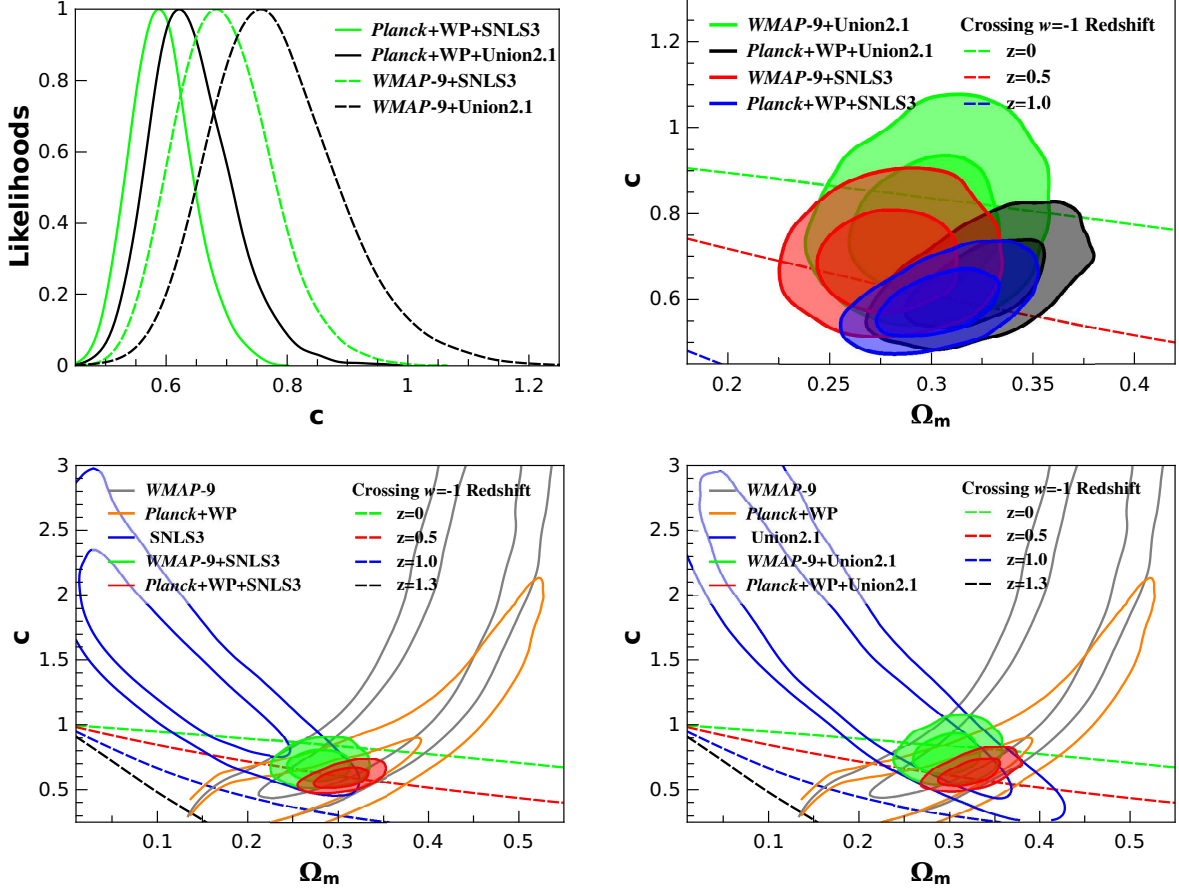


FIG. 11: Fitting results of the HDE model, from CMB combined with BAO and *HST*. The upper-left panel shows the marginalized distributions of c . The other three panels show the marginalized 68% and 95% CL contours in the Ω_m - c plane, including the CMB+SNLS3 results (lower-left), the CMB+Union2.1 results (lower-right), and a comparison of the CMB+SNLS3 and CMB+Union2.1 results (upper-right).

Another interesting phenomenon is that, although there is no severe tension when we combine Union2.1 with BAO+*HST* or *Planck*+WP, evident tension appears when we combine all these data sets together. Table II shows that $\Delta\chi^2_{\text{Planck+WP+lensing+Union2.1+BAO+HST}} = 9.6$, as large as $\Delta\chi^2_{\text{Planck+WP+lensing+SNLS3+BAO+HST}}$ (that is equal to 10.9). This tension mainly comes from the discrepancy between the results of *Planck*+WP+lensing and Union2.1+BAO+*HST*: we find that $\chi^2_{\text{Planck+WP+Union2.1+BAO+HST+lensing}} - \chi^2_{\text{Planck+WP+lensing}} - \chi^2_{\text{Union2.1+BAO+HST+lensing}} = 8.6$. The fitting results of Union2.1+BAO+*HST* are $\Omega_m = 0.326 \pm 0.030$, $c = 0.633 \pm 0.086$ and $H_0 = 73.09 \pm 2.36$, while for *Planck*+WP+lensing the results are

$\Omega_m = 0.248 \pm 0.079$ and $c = 0.508 \pm 0.207$. When we combine them, we get $\Omega_m = 0.281 \pm 0.012$, $c = 0.577 \pm 0.039$ and $H_0 = 70.68 \pm 1.40$. These three sets of results do not match with each other. Especially, the constraint result of H_0 in the all-combined analysis is in tension with the *HST* measurement.

For *WMAP*-9 we find that $\Delta\chi^2_{WMAP-9+SNIa+BAO+HST} = 5.6$ and 4.3 for SNLS3 and Union2.1, respectively, which also implies some tension, but not so severe as the *Planck* case. Thus, it is no longer viable to do an all-combined analysis by combining *Planck* data with all the external data sets of SNIa, BAO and *HST*. Our tightest *self-consistent* constraint is $c = 0.495 \pm 0.039$ obtained from *Planck*+WP+BAO+*HST*+lensing.

V. CONCLUDING REMARKS

In this paper we perform detailed investigation on the constraints on the HDE model by using the *Planck* data. We find the following results:

- HDE provides a good fit to the *Planck* high- ℓ temperature power spectrum. The discrepancy at $\ell \lesssim 20 - 40$ found in the Λ CDM model remains unsolved in the HDE model. The best-fit power spectra of the Λ CDM, w CDM and HDE models are similar to each other at $\ell \gtrsim 25$. In the $\ell \lesssim 25$ region, the w CDM and HDE spectra have slightly lower amplitudes than the Λ CDM spectrum.
- *Planck* data alone can lead to interesting constraint on c . By using *Planck*+WP+lensing, we get $c = 0.508 \pm 0.207$ (68% CL), favoring the present phantom behavior of HDE at the more than 2σ CL. Comparably, by using *WMAP*-9 data alone we cannot get valuable constraint on c .
- In the HDE model, we find $A_L > 1$ at the 2.2σ and 1.7σ levels by using the *Planck*+WP and *Planck*+WP+lensing data. So, HDE cannot help remove or relieve the anomaly of A_L (i.e., the preference for high A_L in the temperature power spectrum).
- At the 68% CL, the results are $c = 0.484 \pm 0.070$, $c = 0.474 \pm 0.049$, $c = 0.594 \pm 0.051$, and $c = 0.642 \pm 0.066$ from *Planck*+WP combined with BAO, *HST*, SNLS3 and Union2.1, respectively. The constraints can be improved by 2%–15% if we further add the *Planck* lensing data into the analysis. The results from *WMAP*-9 combined with each Ext are $c = 0.746 \pm 0.165$, $c = 0.569 \pm 0.086$, $c = 0.696 \pm 0.078$ and $c = 0.782 \pm 0.105$. Compared with *WMAP*-9+Ext results, we find that *Planck*+WP+Ext results reduce the error by 30%–60%, and prefer a more phantom-like HDE.
- Non-standard dark energy models are helpful in relieving the tension between CMB and *HST* measurements. In the CMB-only analysis, the strong correlation between c (w) and $\Omega_m h^3$ in the HDE

(w CDM) model makes H_0 unconstrained. We find that $\chi^2_{Planck+WP+HST} - \chi^2_{Planck+WP} = 7.8, 1.0$ and 0.3 for the Λ CDM, w CDM and HDE models, respectively.

- There is no evident tension when we combine *Planck*+WP with BAO, *HST* or Union2.1: values of $\Delta\chi^2 \equiv \chi^2_{Planck+WP+Ext} - \chi^2_{Planck+WP} - \chi^2_{Ext}$ for them are 1.7, 0.3 and 1.6, respectively. The SNLS3 data set is in weak tension with the other data sets. When SNLS3 is combined with *Planck*+WP, *Planck*+WP+lensing, *WMAP*-9 and BAO+*HST*, we obtain large values of $\Delta\chi^2$, equal to 6.4, 7.3, 3.5 and 4.1, respectively.
- The *Planck*+WP+BAO and *Planck*+WP+*HST* results are in good agreement with each other. The best-fit and 68% CL constraints on H_0 in the *Planck*+WP+BAO analysis are $H_0 = 72.63$ and $H_0 = 75.06 \pm 3.82$, close to the *HST* measurement result, $H_0 = 73.8 \pm 2.4$.
- Although Union2.1 is not in tension with CMB or BAO+*HST*, the combination Union2.1+BAO+*HST* is in tension with the combination *Planck*+WP+lensing. When we combine the two together, we find $\Delta\chi^2 = 8.6$. So it is not viable to do an all-combined analysis for HDE by using the *Planck* data combined with all the Exts. Our tightest self-consistent constraint is $c = 0.495 \pm 0.039$ obtained from *Planck*+WP+BAO+*HST*+lensing.

Acknowledgments

We acknowledge the use of *Planck* Legacy Archive and the discussion with Gary Hinshaw. We thank KIAS Center for Advanced Computation and Institute for Theoretical Physics for providing computing resources. XDL thanks Juhan Kim for valuable discussions and kind help. ZHZ thanks Cheng Cheng for kind help. ML and ZZ are supported by the National Natural Science Foundation of China (Grant Nos. 11275247 and 10821504). XDL is supported by the Korea Dark Energy Search (KDES) grant. YZM is supported by the Natural Sciences and Engineering Research Council of Canada and Canadian Institute for Theoretical Astrophysics (CITA). XZ is supported by the National Natural Science Foundation of China (Grant Nos. 10705041, 10975032 and 11175042), and by the National Ministry of Education of China (Grant Nos. NCET-09-0276, N100505001 and N120505003).

-
- [1] A. G. Riess *et al.*, *AJ*. **116**, 1009 (1998); S. Perlmutter *et al.*, *ApJ*. **517**, 565 (1999).
[2] V. Sahni and A. Starobinsky, *Int. J. Mod. Phys. D***9**, 373 (2000); P. J. E. Peebles and B. Ratra, *Rev. Mod. Phys.* **75**, 559 (2003); T. Padmanabhan, *Phys. Rept.* **380**, 235 (2003); E. J. Copeland, M. Sami and S. Tsujikawa, *Int.*

- J. Mod. Phys. D **15**, 1753 (2006); V. Sahni and A. Starobinsky, Int. J. Mod. Phys. **D15**, 2015 (2006); J. Frieman, M. Turner and D. Huterer, Ann. Rev. Astron. Astrophys **46**, 385 (2008); S. Tsujikawa, arXiv:1004.1493; M. Li *et al.*, Commun. Theor. Phys. **56**, 525 (2011); M. Li *et al.*, arXiv:1209.0922.
- [3] E. Witten, arXiv:hep-ph/0002297.
- [4] G. 't Hooft, gr-qc/9310026; L. Susskind, J. Math. Phys. **36**, 6377 (1995); J. D. Bekenstein, Phys. Rev. D **7**, 2333 (1973); J. D. Bekenstein, Phys. Rev. D **9**, 3292 (1974); J. D. Bekenstein, Phys. Rev. D **23**, 287 (1981); J. D. Bekenstein, Phys. Rev. D **49**, 1912(1994); S. W. Hawking, Commun. Math. Phys. **43**, 199 (1975); S. W. Hawking, Phys. Rev. D **13**, 191 (1976).
- [5] A. Cohen, D. Kaplan, A. Nelson, Phys. Rev. Lett. **82**, 4971 (1999).
- [6] M. Li, Phys. Lett. B **603**, 1 (2004).
- [7] Q. G. Huang and M. Li, JCAP **03**, 001 (2005); X. Zhang, Int. J. Mod. Phys. D **14**, 1597 (2005); Phys. Lett. B **648**, 1 (2007); Phys. Rev. D **74**, 103505 (2006); B. Chen, M. Li and Y. Wang, Nucl. Phys. B **774**, 256 (2007); J. F. Zhang, X. Zhang and H. Y. Liu, Phys. Lett. B **651**, 84 (2007); Eur. Phys. J. C **52**, 693 (2007); C. J. Hogan, astro-ph/0703775; arXiv:0706.1999; H. Wei and S. N. Zhang, Phys. Rev. D **76**, 063003 (2007); M. Li, C. S. Lin and Y. Wang, JCAP **05**, 023 (2008). Y. Z. Ma and X. Zhang, Phys. Lett. B **661**, 239 (2008); M. Li *et al.*, Commun. Theor. Phys. **51**, 181 (2009); B. Nayak and L. P. Singh, Mod. Phys. Lett. A **24**, 1785 (2009); K. Y. Kim, H. W. Lee and Y. S. Myung, Mod. Phys. Lett. A **24**, 1267 (2009); M. Li, R. X. Miao and Y. Pang, Phys. Lett. B **689**, 55 (2010); M. Li, R. X. Miao and Y. Pang, Opt. Express **18**, 9026 (2010); M. Li and Y. Wang, Phys. Lett. B **687**, 243 (2010); Y. G. Gong and T. J. Li, Phys. Lett. B **683**, 241 (2010); L. N. Granda, A. Oliveros and W. Cardona, Mod. Phys. Lett. A **25**, 1625 (2010); X. Zhang, Phys. Lett. B **683**, 81 (2010); Z. P. Huang and Y. L. Wu, arXiv:1202.4228; M. Li and R. X. Miao, arXiv:1210.0966.
- [8] Q. G. Huang and Y. G. Gong, JCAP **08**, 006 (2004); X. Zhang and F. Q. Wu, Phys. Rev. D **72**, 043524 (2005); Phys. Rev. D **76**, 023502 (2007); Z. Chang, F. Q. Wu and X. Zhang, Phys. Lett. B **633**, 14 (2006); Y. Z. Ma, Y. Gong and X. L. Chen, Eur. Phys. J. C **60**, 303 (2009); M. Li *et al.*, JCAP **06**, 036 (2009); M. Li, X. D. Li and X. Zhang, Sci. China Phys. Mech. Astron. **53**, 1631 (2010); Z. H. Zhang *et al.*, JCAP **06**, 009 (2012).
- [9] Y. H. Li, S. Wang, X. D. Li and X. Zhang, JCAP **02**, 033 (2013).
- [10] P. A. R. Ade *et al.*, *Planck* Collaboration, arXiv:1303.5062 [astro-ph.CO].
- [11] P. A. R. Ade *et al.*, *Planck* Collaboration, arXiv:1303.5076 [astro-ph.CO].
- [12] E. Komatsu *et al.*, ApJS. **192**, 18 (2011).
- [13] C. L. Bennett *et al.*, arXiv:1212.5225; G. Hinshaw *et al.*, arXiv:1212.5226.
- [14] J. Guy *et al.*, A&A **523**, A7 (2010); M. Sullivan *et al.*, ApJ **737**, 102 (2011).
- [15] A. G. Riess *et al.*, ApJ. **730**, 119 (2011).
- [16] W. L. Freedman *et al.*, ApJ. **758**, 24 (2012).
- [17] N. Suzuki *et al.*, ApJ **746**, 85 (2012).
- [18] A. Lewis, A. Challinor and A. Lasenby, ApJ **538**, 473 (2000); A. Challinor and A. Lewis, Phys. Rev. D **D84**, 043516 (2011).
- [19] W. Fang, *et al.*, Phys. Rev. D **78** 103509 (2008); W. Fang, W. Hu, and A. Lewis, Phys. Rev. D **78** 087303 (2008).

- [20] A. Lewis and S. Bridle, *Phys. Rev. D* **66**, 103511 (2002).
- [21] A. Gelman and D. Rubin, *Statistical Science* **7**, 457 (1992).
- [22] *Planck* Collaboration, arXiv:1303.5077.
- [23] S. Das *et al.*, arXiv:1301.1037; R. Keisler *et al.*, *ApJ* **743** 28 (2011); C. L. Reichardt *et al.*, *ApJ* **763**, 127 (2013); C. L. Reichardt *et al.*, *ApJ* **755**, 70 (2012); K. T. Story *et al.*, arXiv:1210.7231.
- [24] W. Hu, *ASP Conf. Ser.* **339**, 215 (2005).
- [25] S. Cole *et al.*, *MNRAS* **362**, 505 (2005).
- [26] N. Padmanabhan *et al.*, *MNRAS* **427**, 2132 (2012).
- [27] L. Anderson *et al.*, *MNRAS* **428**, 1036 (2013).
- [28] J. Guy *et al.*, *A&A* **466**, 11 (2007).
- [29] A. J. Conley *et al.*, *ApJ* **681**, 482 (2008).
- [30] G. E. Addison, G. Hinshaw and M. Halpern, arXiv:1304.6984.
- [31] E. Calabrese *et al.*, *Phys. Rev. D* **77**, 123531 (2008).